Journal of Advanced Research 80 (2026) 759–773

Contents lists available at ScienceDirect

Journal of Advanced Research

journal homepage: www.elsevier.com/locate/jare

Original Manuscript

Hyperoside modulates bile acid and fatty acid metabolism, presenting a potentially promising treatment for non-alcoholic fatty liver disease

Songsong Wang [a,1,*], Qiang Jia [b,1], Xiaoli Liu [a,b], Yihan Ma [a], Ying Yang [a], Xue Rong [b], Yang Wang [d], Haiyang Wang [a,c], Fusheng Liu [c], Shenshen Yang [e], Yubo Li [a,e], Liwen Han [a,*]

[a] School of Pharmaceutical Sciences & Institute of Materia Medica, Shandong First Medical University & Shandong Academy of Medical Sciences, Jinan 250117 Shandong, China
[b] Institute of Pharmaceutical Research, Shandong Key Laboratory of Digital Traditional Chinese Medicine, Shandong University of Traditional Chinese Medicine, Jinan 250355, China
[c] State Key Laboratory Base of Eco-chemical Engineering, College of Chemical Engineering, Qingdao University of Science and Technology, Qingdao 266042, China
[d] Jilin Ginseng Academy, Changchun University of Chinese Medicine, Changchun 130117, China
[e] School of Chinese Materia Medica, Tianjin University of Traditional Chinese Medicine, Tianjin 301617, China

HIGHLIGHTS

- Hyperoside activates hepatic FXR, thereby alleviating NAFLD in rats.
- Hyperoside inhibits hepatic ACLY independently of FXR, working synergistically with activated FXR to suppress fatty acid synthesis.
- Hyperoside increases conjugated BAs in rat ileum by by inhibiting BSH bacteria.

GRAPHICAL ABSTRACT

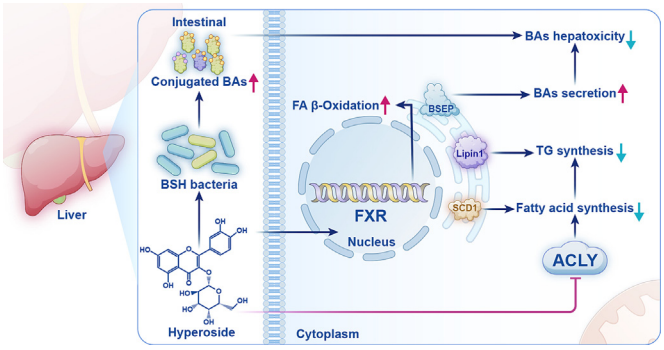

ARTICLE INFO

Article history:
Received 12 February 2025
Revised 3 May 2025
Accepted 8 May 2025
Available online 9 May 2025

Keywords:
Non-alcoholic fatty liver disease
Hyperoside
Farnesoid X receptor
ATP Citrate Lyase
Bile acids metabolism
Fatty acid metabolism

ABSTRACT

Introduction: Non-alcoholic fatty liver disease (NAFLD) is a multifactorial chronic condition that requires a systematic approach for effective management. Multi-effect therapeutic drugs derived from traditional Chinese medicine are increasingly being recognized as promising alternatives for NAFLD intervention. Hyperoside, a natural flavone glycoside found in *Cuscuta chinensis Lam*, *Forsythia suspensa*, and *Crataegus pinnatifida Bge*, has been shown to effectively mitigate NAFLD in rats. However, the underlying mechanism through which hyperoside alleviates NAFLD remains unclear.
Objective: This study aims to explore the specific mechanisms by which hyperoside intervenes in the progression of NAFLD.
Methods: In this study, a high-fat diet was used to induce the NAFLD model in rats. An integrated analysis, including mass spectrometry-based lipidomics, TMT-based proteomics, 16S rRNA sequencing, and bile acid-targeted metabolomics, was employed to identify significantly altered metabolites and proteins. Western blotting, molecular docking, and isothermal titration calorimetry were conducted to analyze the direct targets of action.
Results: The results indicate that hyperoside activates farnesoid X receptor (FXR), promoting fatty acid oxidation and the efflux of bile acids from the liver. Additionally, hyperoside inhibits hepatic ATP citrate lyase (ACLY) and works synergistically with activated FXR to suppress *de novo* lipogenesis. Hyperoside also inhibits intestinal microbes linked to bile-salt hydrolase (BSH) activity, which enhances the

* Corresponding authors at: No. 6699 Qingdao Road, Huaiyin Distinct, Jinan, PR China.
E-mail addresses: wangsongsong@sdfmu.edu.cn (S. Wang), hanliwen@sdfmu.edu.cn (L. Han).
[1] These authors contributed equally to this work.

https://doi.org/10.1016/j.jare.2025.05.014

production of ileal bile acids (BAs), particularly conjugated BAs, thus reducing the liver toxicity of endogenous BAs.

Conclusion: Our findings suggest that hyperoside alleviates NAFLD by modulating fatty acid and bile acid metabolism through FXR and ACLY, suggesting its potential as a multi-effect candidate drug for the treatment of NAFLD.

Introduction

Non-alcoholic fatty liver disease (NAFLD) is a prevalent chronic hepatic disorder worldwide, characterized by the accumulation of lipid droplets in more than 5 % of hepatocytes. It encompasses a range of conditions, including nonalcoholic fatty liver, nonalcoholic steatohepatitis, and fibrosis [1,2]. Over the past 20 years, the understanding of NAFLD pathogenesis has evolved from the "two-hit theory" to the "multiple-hit model", which primarily involves hepatic triglyceride accumulation, inflammatory cytokines, mitochondrial dysfunction, and widespread metabolic disturbances[3,4]. However, liver triglyceride accumulation is considered the "initial trigger" [5,6]. Hepatic triglyceride levels are largely influenced by the uptake of free fatty acids, *de novo* lipogenesis, fatty acid oxidation, and VLDL secretion. NAFLD develops when the liver fails to adequately compensate for the increased uptake of circulating fatty acids and the *de novo* synthesis of lipids [7,8]. Due to the complex pathogenesis of NAFLD, only one pharmacological treatment has been approved by FDA, underscoring the critical need for discovering new multi-effect therapeutic approaches [9].

The farnesoid X receptor (FXR), a nuclear receptor, regulates of bile acids (BAs), as well as lipid and glucose metabolism, and is physiologically activated by BAs. Numerous studies suggest that FXR activation may also alleviate hepatic fibrosis and inflammation by modulating downstream target genes, thus exerting therapeutic effects to NAFLD. For instance, the FXR activation can inhibit CYP7A1, the key enzyme in BAs synthesis, both directly and indirectly, thereby reducing BAs production. This decrease in BAs synthesis mitigates the hepatotoxicity of endogenous BAs and contributes to liver protection. However, interventions targeting FXR are associated with significant side effects and poor efficacy [10], including pruritus and disrupted cholesterol metabolism [11,12]. Therefore, a single-target drug for treating NAFLD may not be sufficient to reverse the entire disease process. As a result, multi-effect drugs with various pharmacological mechanisms are gradually becoming a research focus, as they are expected to enhance efficacy and reduce adverse reactions, making them a promising therapeutic option for NAFLD.

Traditional Chinese medicine (TCM) is widely recognized as a complementary and alternative approach to managing NAFLD [13,14]. Its extracts are considered promising candidates for multi-target therapeutic agents that can prevent and treat NAFLD by modulating various pathways, including inflammation, insulin sensitivity, lipid metabolism, mitochondrial dysfunction, intestinal microbiota, and autophagy [15–17]. The active ingredients of TCM exhibit characteristics such as multi-targeting, multi-pathway interactions, and low selectivity, offering significant advantages in the intervening and treating NAFLD, which is characterized by complex pathological mechanisms[18,19]. Numerous therapeutic agents derived from TCM, such as silibinin, curcumin, and resveratrol, have been extensively studied for their diverse effects and targets[20,21]. Therefore, compounds from TCM have emerged as a valuable source for discovering anti-NAFLD drugs.

Hyperoside, a natural flavonol glycoside found in several plants, including *Cuscuta chinensis Lam*, *Forsythia suspensa*, and *Crataegus pinnatifida Bge*, exhibits a broad range of biological activities[22]. These include anticancer, antidepressant, anti-inflammatory, antibacterial, hepatoprotective, and antiviral effects [23]. An acute toxicity test of hyperoside revealed an LD50 greater than 5000 mg/kg, indicating a low potential for toxicity in organisms [24]. In our previous study, we were the first to demonstrate that hyperoside effectively improves NAFLD by reversing steatosis [25]. However, the molecular mechanism through which hyperoside combats NAFLD remains to be fully understood. In present study, we sought to elucidate the underlying mechanism by which hyperoside ameliorates NAFLD, utilizing an integrated TMT proteomics and lipidomics approach. Our findings show that hyperoside activates FXR, promoting BAs efflux from the liver, inhibiting *de novo* lipogenesis, and enhancing fatty acid oxidation. Furthermore, hyperoside suppresses hepatic ATP citrate lyase (ACLY), working in synergy with activated FXR to inhibit *de novo* lipogenesis. Additionally, hyperoside can inhibit the activity of bile salt hydrolase bacteria, reducing the deconjugation of conjugated BAs. Our findings further support the potential of hyperoside as a promising novel therapeutic agent for the treatment of NAFLD.

Materials and methods animals and experimental protocol

For the experimental procedures, 10-week-old male Wistar rats were procured Pengyue Experimental Animal Breeding (Jinan, China). All animals were housed in the College of Pharmacy, Shandong First Medical University (Jinan, China). The rats were separately kept in ventilated squirrel cages with controlled environmental conditions (humidity 60 ± 5 %, 22 ± 2℃, and a 12-h light/dark cycle). They were provided with either a basic diet (Control group) or a specific high-fat diet (HFD, model group; TROPHIC Animal Feed High-Tech, Nanjing, China). The HFD comprised 66 % basic feed diet, 20 % lard, 12 % sucrose, and 2 % cholesterol, and was stored at 4℃ until use. Additionally, hyperoside group received a high-fat diet mixed with hyperoside. Following the final administration and anesthesia, and serum and liver samples were harvested and stored at −80℃ for subsequent analysis.

Ethics statement

The animal study was approved by The Animal ethics committee of Shandong First Medical University(S6066) and conducted in accordance with their principles.

16S rRNA gene sequences

The total genomic DNA was isolated using the OMEGA-Soil-DNA-Kit (M5635-02) from Omega Bio-Tek, GA, USA. The purity and yield of the DNA samples were examined by agarose gel electrophoresis and NanoDrop 2000c spectrophotometer from Thermo-Fisher-Scientific, MA, USA, respectively. To amplify the 16S rRNA gene V3-V4 region of the DNA samples, forward primer 338F (5′-ACTCCTACGGGGGGCAG-3′) and reverse primer 806R (5′-GACTACHVGGGTWTCTAAT-3′) were used. To enable multiplex sequencing, the primers were incorporated with sample-specific 7-bp barcodes. PCR was carried out as follows: 5 min at 98 °C, followed by 25 cycles of 30 s at 98 °C, 30 s at 53 °C, and 45 s at

72 °C, and then 5 min at 72 °C. The PCR product was purified and used for library construction. The constructed libraries underwent quality testing and were subjected to high-throughput sequencing on the Illumina NovaSeq platform using the NovaSeq-6000-SP-Reagent-Kit (500 cycles) at Metabo-Profile Biotechnology (Shanghai, China). QIIME2 2019.4. was used to performe the microbial bioinformatics analysis.

Intestinal BAs analysis

The quantitative analysis was performed based on a previous study with some modifications [25]. Fecal samples weighing 10 mg were collected and placed in Eppendorf Safe-Lock tubes. To these tubes, 25 mg of pre-cooled grinding beads and 200 μL of an acetonitrile/methanol solution (*v*/*v* = 8:2) containing 10 μL of internal standard were added. The mixture was homogenized and centrifuged at 13,500 rpm for 20 min at 4 °C using a Microfuge 20R (Beckman Coulter, IN, USA). Subsequently, 10 μL of the supernatant was isolated and diluted with 90 μL of a 1:1 mixture of ultrapure water and acetonitrile/methanol (*v*/*v* = 8:2). Following oscillation and centrifugation, and the prepared samples were ready for detection (injection volume = 5 μL). For quantitation of the BAs, an Ultra-performance liquid chromatography/-tandem mass spectrometry (UPLC-MS/MS) system (ACQUITY UPLC-Xevo TQ-S, Waters Corp., MA, USA) was employed. The analytical column used was an ACQUITY UPLC Cortecs C18 with a particle size of 1.6 and a column temperature of 30 °C. Phase A contained water with formic acid (pH = 3.25), and phase B contained a mixture of acetonitrile/methanol (80:20). The gradient conditions were as follows: 5 % B (0–1 min), 5–30 % B (1–3 min), 30–100 % B (3–15 min), 100–5 % B (15–16 min), and 5 % B (16–17 min). The flow rate was set at 0.4 mL/min, with an injection volume of 5.0 μL. The mass spectrometer was operated under the following parameters: capillary voltage (Kv) = 2.0 (ESI-), source temperature = 150 °C, and desolvation temperature = 5 50 °C. The desolvation gas flow was set at 1000 L/Hr. The raw data collected from the UPLC-MS/MS system were analyzed using QuanMET software (v2.0, Metabo-Profile, Shanghai, China).

Serum lipidomics analysis

The serum samples (100 μL) were transferred to tubes and mixed with 480 μL methanol: MTBE (1:5). The samples were vortexed for 60 s and then sonicated for 10 min in a 4℃ water bath. After incubating at −40℃ for 1 h, they were centrifuged at 3,000 rpm for 15 min at 4℃. The supernatant obtained was dried in 37℃ vacuum concentrator, followed by reconstitution in 100 μL methanol (50 %) in dichloromethane. The samples were then vortexed for 30 s, sonicated for 10 min, and centrifuged (12,000 rpm, 15 min, 4℃). The resulting supernatant (75 μL) was taken for LC/MS analysis. For quality control, equal aliquots of 20 μL were taken from the supernatants of all samples and combined into a single pool.

LC-MS/MS analysis was conducted using an UHPLC system (1290, Agilent Technologies) coupled to a Kinetex C18 column (1.7 μm, 2.1 × 100 mm, Phenomen). The mobile phase A contained 60 % acetonitrile, 40 % water, and 10 mmol/L ammonium formate, while the mobile phase B was composed of 90 % isopropanol and 10 % acetonitrile, with the addition of 50 mL of 10 mmol/L ammonium formate per 1000 mL of mixed solvent. The elution gradient was as follows: 40 % B (0–1.5 min); 40 %-85 % B (1.5–10.5 min); 85 % B (10.5–14.0 min); 85 %-100 % B (14.0–14.1 min); 100 % B (14.1–15.0 min); 100 %-40 % B (15.0–15.2 min); 40 % B (15.2–18.0 min). The auto-sampler temperature, column temperature and injection volume were 4 °C, 55 °C and 2.0 μL, respectively.

The detailed parameters for the Pro mass spectrometer during full MS and MS/MS data collection were as follows: sheath gas flow = 12 L/min, sheath gas temperature = 350 °C; dry gas flow = 8 L/min; dry gas temperature = 325 °C; capillary voltages, +3.5 kV and −3.5 kV for positive and negative modes, respectively. The exit and entrance voltages of the drift tube were 250 V and 1,700 V, respectively. Trap release and filling times were 150 μs and 20,000 μs, respectively. The maximum drift time was 60 ms, and the mass range was from 100 to 1,700 Da. During frame 2, MS/MS data acquisition was conducted using all ion fragmentation (AIF) with a collision energy set at 30 V.

The raw data were converted to mzXML format with ProteoWizard. Peak detection, extraction, alignment, and integration were performed using the CentWave algorithm in XCMS, with the cutoff of 0.6, for annotation. To identify lipids, spectral matching was performed using the lipid IMMS library.

Hepatic TMT-based proteomics analysis

Liver tissue was lysed and homogenized using 200 μL of lysis buffer. The homogenate was heated for 5 min, followed by ultrasound treatment, and heated again for 5 min. Liver protein specimens were obtained by centrifugation at 16,000 rpm for 15 min and quantified using a BCA Protein Assay Kit (Bio-Rad, USA).

Protein digestion (200 μg) was conducted following the FASP protocol. In brief, the detergent, DTT, and other low-molecular-weight compounds were removed using 200 μL of UA buffer through repeated ultrafiltration (Microcon units, 30 kD) facilitated by centrifugation. After that, 100 μL of iodoacetamide (0.05 M) in UA buffer was introduced to inhibit reduced cysteine residues, followed by incubation for 20 min in the dark. The filter was rinsed three times with UA buffer (100 μL) and twice with 25 mM NH_4HCO_3 (100 μL). The protein suspension was then enzymatically digested overnight at 37 °C with 4 μg of trypsin (Promega) in 40 μL of 25 mM NH_4HCO_3. The concentration of the resulting peptides was measured using a Nanodrop, with absorbance assessed at 280 nm.

Peptides were subjected to TMT labeling (Thermo-Fisher-Scientific). Each aliquot (100 μg of peptides) was mixed with an individual tube of TMT reagent. The peptide sample and TMT reagent were dissolved in 100 μL of 0.05 M TEAB solution and 41 μL of anhydrous acetonitrile, respectively. After one hour of incubation, 8 μL of 5 % hydroxylamine was added, and the mixture was incubated for an additional 15 min. The multiplex-labeled peptides were then combined and subjected to lyophilization.

The pierce high pH reversed phase peptide fractionation kit (Thermo-Fisher-Scientific) was used to fractionate the multiplex-labeled peptides. After conditioning the spin column, 100 μg of TMT-labeled peptides was dissolved in 300 μL 0.1 % TFA solution. The sample solution was loaded onto the spin column and centrifuged at 3000 × g for 2 min. The eluate from this process was retained as the "flowthrough" fraction. Similarly, the same procedure was applied with Milli-Q water to collect the "wash" fraction. To eliminate unreacted TMT reagent, the TMT-labeled peptides underwent an additional column wash with 300 μL of 5 % CAN and 0.1 % trimethylamine. The peptides were then collected, evaporated to dryness, and subsequently stroed at −80 °C.

The resulting LC-MS/MS raw data were processed using MaxQuant software (v 1.6.0.16) for data interpretation and proteins identification. The identification process involved searching against the Uniprot_Hordeum-vulgare_201747-20180125 database, which contains 201,747 protein sequences and was downloaded on 25/01/2018. The preliminary search was configured with 6 ppm window for the precursor mass. The search utilized the enzymatic cleavage rule of Trypsin/P and permitted up to two potential missed cleavage sites. For fragment ions, a mass tolerance of 20 ppm was permitted. The modification set used for the search included fixed modifications such as Carbamidomethyl (C), TMT10plex (K), and TMT10plex (N-term). Additionally, variable

modifications such as Oxidation(M) and Acetyl (Protein N-term) were considered. For peptide and protein identification, a minimum of 6 amino acids per peptide and at least one unique peptide per protein were required. The false discovery rate (FDR) was 1 % for both protein and peptide identification. Protein quantification was conducted using TMT reporter ion intensity.

Western blot analysis

Liver and cell samples (20 mg) were lysed in RIPA lysis buffer (Beyotime, China) containing 1 % protease inhibitor cocktail (Abmole, USA). The total protein lysates were separated on 10 % SDS-PAGE gels and subsequently transferred to PVDF membranes. These membranes were incubated overnight at 4 °C with primary antibodies specific to FXR (ABclonal), CD36 (ABclonal), ACLY (ABclonal), ACSL1 (ABclonal), FGF15(ABclonal), GAPDH (ABclonal). Following incubation with HRP-conjugated secondary antibodies (ABclonal), protein bands were visualized using an ECL Plus immunoblot detection system (Tanon 5200) and quantified with Image Jet software.

Statistics

Data quantification was performed blindly and presented as mean ± standard error of mean (SEM) utilizing GraphPad Prism software (version 9.0). Two-tailed Student's *t* test was used for two group comparisons between two groups. For dataset with more than two groups, one-way ANOVA was employed. A p-value of less than 0.05 was deemed statistically significant.

Results

Hyperoside reduced hepatic lipid levels and maintained serum lipid homeostasis in NAFLD rats

Male Wistar rats were subjected to two different diets for 8 weeks: a basic chow and a high-fat diet (HFD group). Within the HFD group, half of the rats received hyperoside (Hyp) aqueous solution at doses of 1.5 mg/kg and 3.0 mg/kg (HFD + Hyp 1.5 mg/kg and HFD + Hyp 3.0 mg/kg). After 6 weeks, HE staining of liver tissues from the model group revealed numerous vacuoles and irregular liver cell arrangements. Hyperoside treatment significantly improved common hepatocyte hydropic degeneration and cell swelling. Oil Red O staining of liver tissues indicated aggravated lipid deposition in the HFD group, while hyperoside treatment remarkably reduced the number of lipid droplets, as shown in Fig. 1A-B. HFD rats exhibited significant increases in liver total cholesterol (TC), triglycerides (TG), liver apolipoprotein C (Apo C), Apo E, Apo B, liver very low-density lipoprotein (VLDL), as well as elevated serum levels of Apo C, Apo B, Apo E, and liver VLDL. Serum VLDL was also significantly increased in HFD rats, whereas serum and liver Apo A were significantly decreased. However, serum TC in the HFD group did not significantly differ from the Control group. Hyperoside administration significantly reduced serum and hepatic TG levels and slightly decreased hepatic TC. Moreover, hyperoside treatment markedly decreased elevated levels of liver and serum Apo C, Apo B, Apo E, and VLDL induced by the HFD. Hyperoside also effectively reversed the reduced levels of serum and liver Apo A in the HFD group, as shown in Fig. 1C-D.

TMT-based proteomics revealed that hyperoside activated FXR, promoting the secretion of BAs from the liver to the intestine

TMT-based proteomics was employed to explore the mechanism by which hyperoside alleviates NAFLD. Liver tissue samples from Control, HFD and hyperoside-treated groups were analyzed to identify protein biomarkers involved in hyperoside's therapeutic effect on NAFLD. A total of 5786 proteins were identified, all of which had quantitative information. Differentially expressed proteins were identified based on a fold change of less than 0.83 or greater than 1.2, and with a p-value of less than 0.05. Compared to the HFD group, the hyperoside-treated group exhibited 18 upregulated proteins and 54 downregulated proteins (Fig. 2A). KEGG analysis revealed that the upregulated proteins significantly affected primary BA biosynthesis, taurine and hypotaurine metabolism, the PPAR signaling pathway and others (Fig. 2B). Downregulated proteins significantly affected the MTOR signaling pathway, fatty acid metabolism, biosynthesis of unsaturated FAs, and AMPK signaling pathway, among others. Detailed information on enriched pathways is listed in Table S1. Following hyperoside treatment, levels of sterol 12α-hydroxylase (CYP8B1, cytochrome P450 family 8 subfamily B polypeptide 1) were significantly increased, while ATP citrate lyase (Acly) levels were significantly decreased. Consequently, we further investigated hyperoside's binding to FXR and examined BAs expression profiles post treatment. Hyperoside significantly increased FXR protein expression in both liver and intestines (Fig. 2D).

To confirm FXR as hyperoside's direct target, isothermal titration calorimetry (ITC) and molecular docking experiments were conducted. Hyperoside exhibited a significantly higher binding affinity to FXR, with a dissociation constant (Ka) of 6.65e8 M^{-1}, as illustrated in the Fig. 2J. The molecular docking results indicated stable hydrogen bonds between hyperoside and specific FXR amino acid residues TRY366 and HIS444, with a binding energy −7.5 kcal/mol (Fig. 2F). Molecular dynamics simulations further assessed the stability of the FXR-hyperoside complex. The protein RMSD fluctuated between 3.2 Å and 3.6 Å, stabilizing after 10 ns, while the ligand RMSD remained within 1Å post-10 ns, indicating a stable conformation (Fig. 2G). RMSF analysis revealed interactions in regions exhibiting fluctuations greater than 2Å (Fig. 2H). The radius of gyration (RG) remained within a 1 Å fluctuation throughout the simulation (Fig. 2I). Thus, the FXR-hyperoside complex demonstrated strong binding and stability. Additionally, HepG2 cells treated with TUDCA, an FXR inhibitor, showed a significant reduction in FXR protein expression, which hyperoside effectively reversed, as shown in the Fig. 2E.

FXR activation inhibits BAs synthesis by decreasing CYP7A1 activity while promoting BAs efflux from the liver by increasing BSEP expression. Key proteins involved in BAs synthesis and secretion were analyzed using TMT proteomics. Results indicated no significant changes in key enzymes such as CYP7A1 and CYP27A1 involved in BAs synthesis (Fig. 2C). Metabolomics analysis targeting BAs demonstrated hyperoside treatment reduced serum total BAs concentrations, including unconjugated BAs. Levels of HDCA、NorDCA、TαMCA、ACA、UDCA、7-ketoLCA、αMCA、βMCA、muroCA、CDCA、LCA, and 6-ketoLCA were all decreased compared to the model group (Fig. 2K). These findings align with previous studies showing hyperoside's ability to reduce total and unconjugated BAs levels in the liver and serum of NAFLD model rats, thus mitigating the hepatotoxicity associated with unconjugated BAs. To further investigate BAs secretion post-FXR activation by hyperoside, protein expression associated with BAs secretion was analyzed using heat map analysis. Results indicated increased expression of proteins responsible for BAs secretion, including multidrug resistance-associated protein 4 (MRP4), recombinant multidrug resistance protein 3 (MDR3), and bile salt export pump (BSEP), following hyperoside administration (Fig. 3A). Western blot assays confirmed that hyperoside significantly increased BSEP protein expression of BSEP (Fig. 3B). Moreover, BAs levels in intestinal contents confirmed increased conjugated and total BAs levels post-hyperoside intervention. Among the 45 detected BAs, 20 BAs,

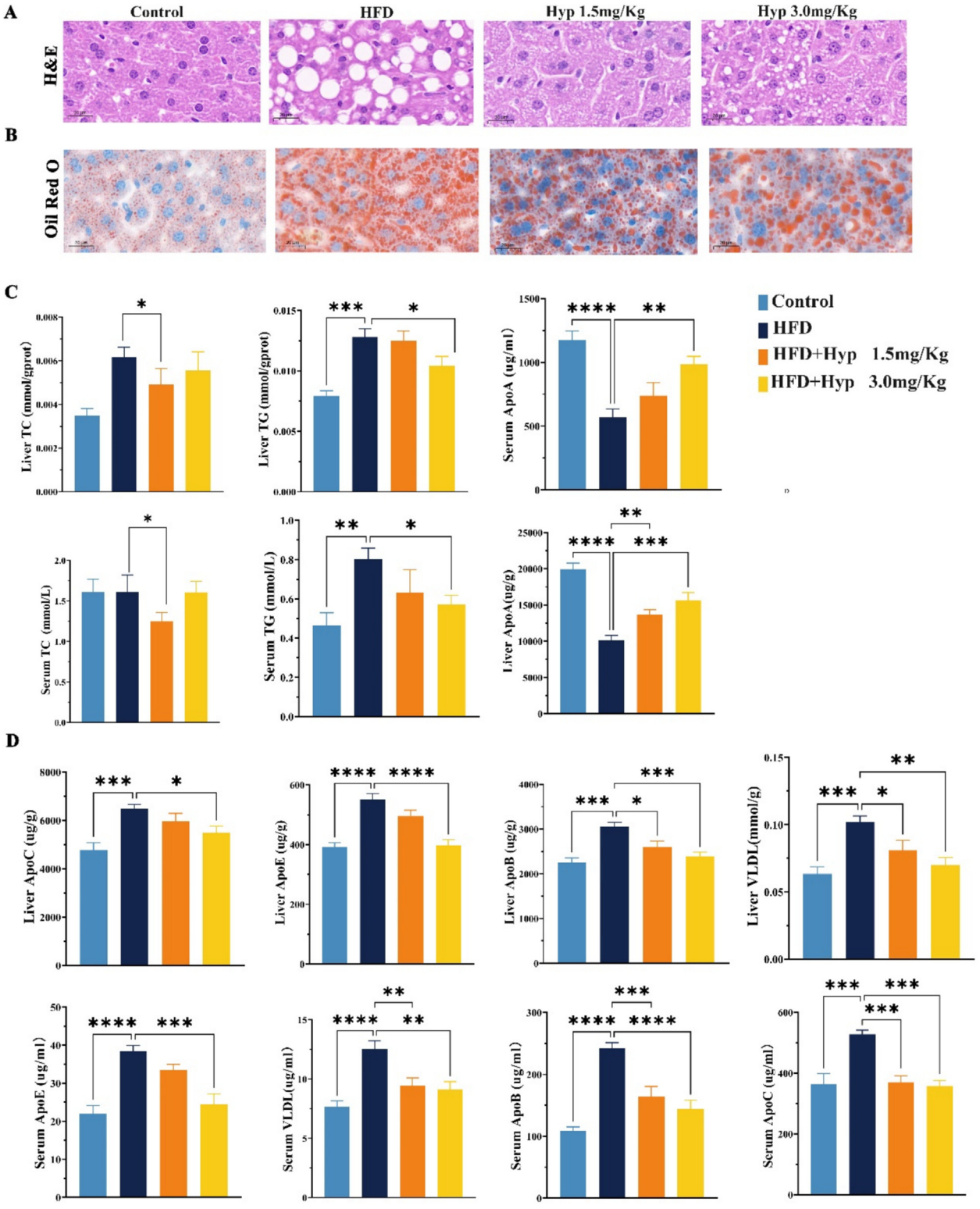

Fig. 1. Liver and Serum lipid lowering effects of hyperoside. A. Representative images of liver tissues stained with HE staining (×40). B. Representative images of liver tissues stained with ORO staining (×40). C. Hyperoside reduced the liver and the serum TC, TG, and AopA. D. Hyperoside reduced the liver and the serum Aop/B/C/E and VLDL. n = 9 individuals/group. Data were expressed as mean ± SEM. Differences of data in rats were assessed by the One-way ANOVA test, respectively, $^{*}P < 0.05$, $^{**}P < 0.01$, $^{***}P < 0.001$.

including TCA, THDCA, GCA, GHDCA, GCDCA, and GDCA, were elevated in the intestinal contents post-hyperoside intervention (Fig. 3C-G). These results indicate that hyperoside, through FXR activation, enhances BAs efflux from the liver rather than significantly reducing BAs synthesis.

Hyperoside reversed the intestinal microbiota disorder in NAFLD rats

BAs metabolism is closely linked to gut microbiota. We aimed to investigate whether hyperoside's regulation of BAs is associated with intestinal flora. To this end, we analyzed the effects of hyper-

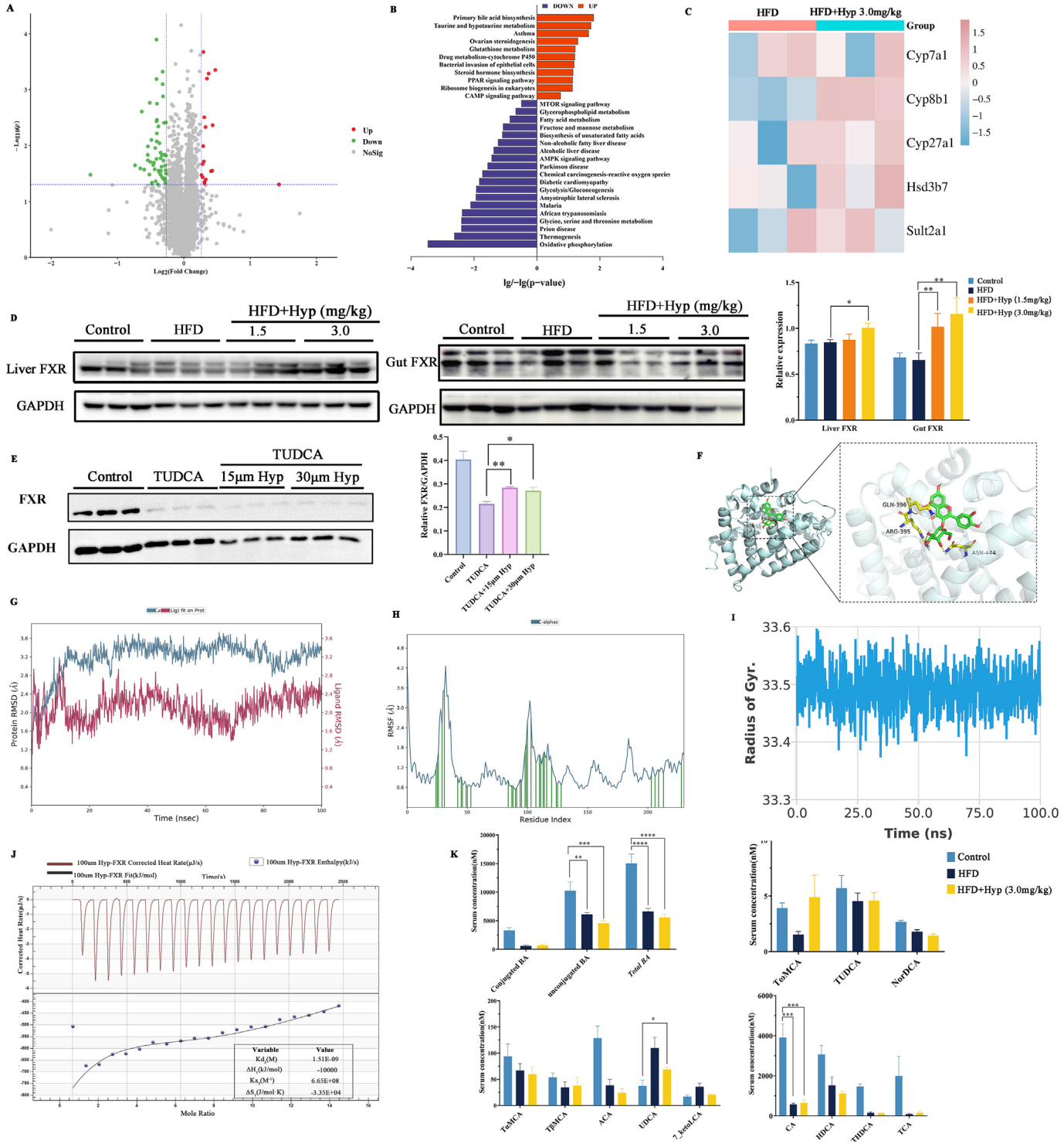

Fig. 2. TMT-based proteomics revealed that hyperoside activates FXR, thereby regulating BAs metabolism. A. a Volcano map of differential proteins between HFD and hyperoside groups. FC > 1.2 or < 0.83, and p < 0.05. B. The KEGG pathway analysis based on the differential proteins between HFD and hyperoside groups. C. The expression of proteins involved in BAs biosynthesis based on TMT-based proteomic analysis. D. Hyperoside elevated protein expression of hepatic and intestinal FXR. E. Hyperoside reversed TUDCA-induced downregulation of FXR expression at the cellular level. F. The stable hydrogen bonds formed between hyperoside and the specific amino acid residues TRY366 and HIS444 of the FXR, providing specific binding energy −7.5 kcal/mol. G. The tendency of the root mean square deviation (RMSD) plot for FXR and Hyperoside complexes. H. FXR's Root Mean Square Swing (RMSF) chart trend. I. FXR's radius of turn (RG) chart trend. J. Isothermal titration calorimetry of FXR with hyperoside. Heat flow as a function of time (red) and the blue dotted line corresponds to the theoretical independent model. Thethermodynamic constants are presented in the pane. K. Serum BAs profile of rat after hyperoside consumption for 8 weeks. n = 7 individuals/group. Differences between data were assessed by the One-way ANOVA test, respectively, $^{*}P < 0.05$, $^{**}P < 0.01$, $^{***}P < 0.001$. (For interpretation of the references to colour in this figure legend, the reader is referred to the web version of this article.)

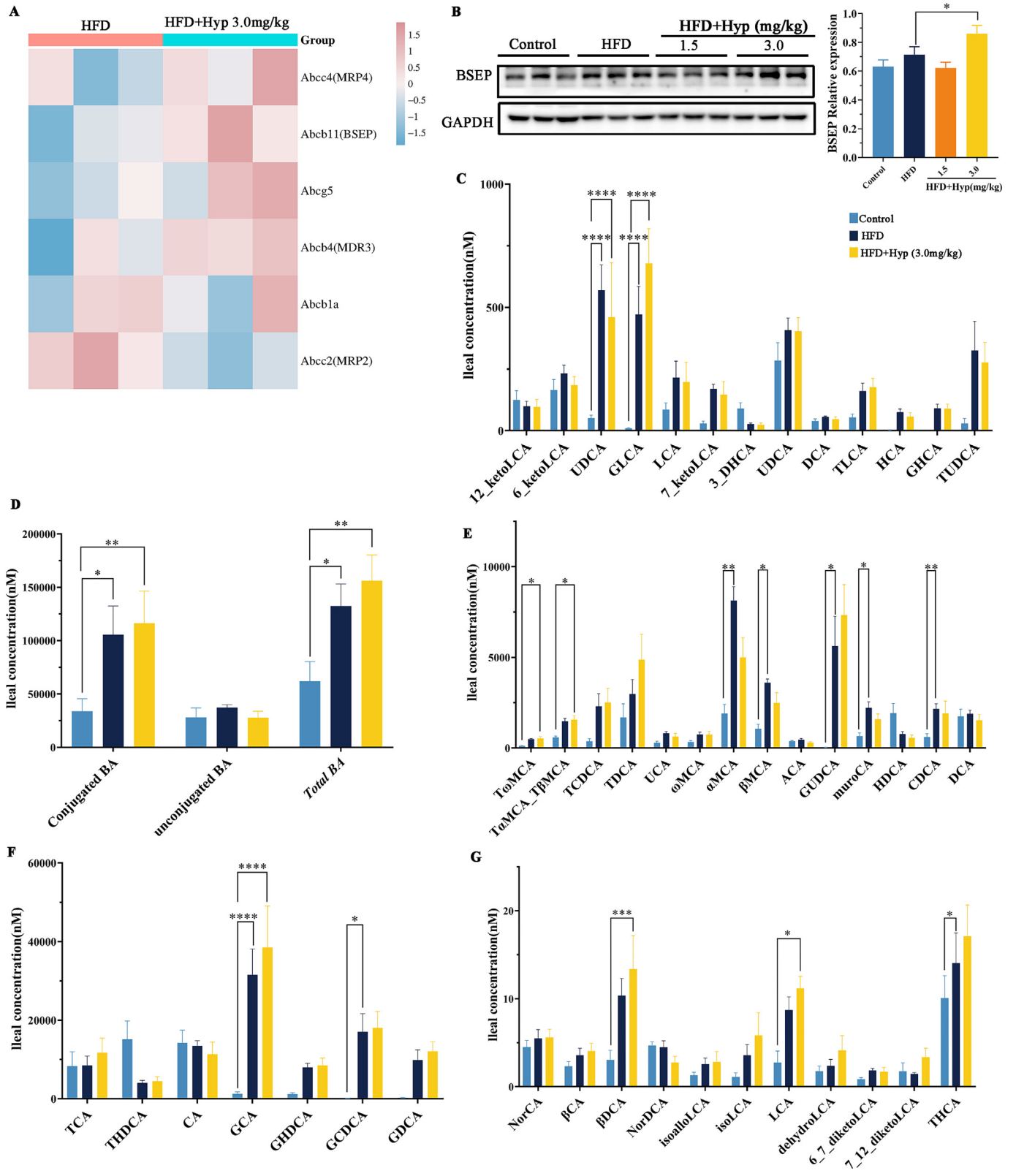

Fig. 3. Hyperoside activates FXR, promoting the secretion of BAs from the liver to the intestine. A. The protein involved in BAs was increased after hyperoside intervention based on TMT-based proteomics. B. The protein expression of hepatic BSEP was significantly increased by hyperoside. C-G. Ileum BAs profile and total BAs of rat after hyperoside consumption for 8 weeks. n = 7 individuals/group. Data were expressed as mean ± SEM. Differences of data in rats were assessed by the One-way ANOVA test, respectively, $^{*}P < 0.05$, $^{**}P < 0.01$, $^{***}P < 0.001$.

oside on gut microbiota using 16S rRNA gene sequence analysis. Microbial samples were collected from the ileum of rats in the Control, HFD, and HFD + Hyp groups. Principal coordinates analysis (PCoA) based on UniFrac distances revealed distinct clustering of gut microbial communities among the groups. Hyperoside treatment led to significant changes in the community structure of rat fecal microbes, as shown in Fig. 4A. LEfSe analysis indicated common alterations in the abundances of different taxonomic levels, as depicted in Fig. 4B, with an increased representation of the Chloroplast class, MBA08 order, and Streptophyta order. Conversely, the relative abundance of various taxa within the Proteobacteria phylum, Chloroflexi phylum, Gammaproteobacteria class, Flavobacteriia class, Anaerolineae class, Pasteurellales order, Flavobacteriales order, MND1 order, Pseudomonadales order, and Pasteurellaceae, Flavobacteriaceae, Enterococcaceae, Pseudomonadaceae, and Bacteroidaceae families, as well as the Aggregatibacter, Faecalibacterium, Enterococcus, Bacteroides, and Pseudomonas genera were reduced in the hyperoside- treated groups. Notably, the reduced Enterococcus and Bacteroides genera are involved in generating bile salt hydrolase (BSH), which deconjugates glycine- or taurine-conjugated BAs to form unconjugated BAs. Additionally, other BSH-producing genera such as Bacillus, Lactobacillus, Lactococcus, Streptococcus, Bifidobacterium, and Clostridium, were also diminished by hyperoside treatment in rats, as shown in Fig. 4E-H. This decrease in BSH-positive bacteria was significant in both rodents and humans. Simultaneously, we assessed BSH activity in serum and found that hyperoside treatment reduced BSH activity in the serum of NAFLD model rats (Fig. 4C). These findings suggest that hyperoside inhibits BSH bacterial activity and decreases BSH production, thereby preventing the breakdown of conjugated BAs and increasing their levels in the organism.

Activation of FXR by hyperoside promotes fatty acid oxidation and de nove lipogenesis

In addition to promoting the secretion of BAs from the liver to the intestine, FXR activation also inhibits lipogenesis and promotes fatty acids oxidation. We employed TMT-based proteomics to investigate the expression of key proteins associated with the SREBP1, fatty acid synthesis, and PPAR oxidation pathways. The results indicated that.

hyperoside decreased the expression of proteins involved in triglyceride synthesis and AMPK target proteins (Fig. 5A-B). Conversely, hyperoside increased the expression of proteins associated with fatty acid decomposition and oxidation (Fig. 5C-D). The downregulation of SCD1 and LIPIN1 may be related to FXR activation. Using Western Blot technology, we detected the levels of SCD1, LIPIN1, and CPT1/2. The results were consistent with our proteomics data, revealing that hyperoside significantly decreased the protein expression of SCD1 and LIPIN1 while increasing CPT1/2 protein expression, as illustrated in Fig. 5E-G. These findings suggest that hyperoside activates FXR, thereby reducing liver lipids by inhibiting fatty acid and lipid synthesis while promoting fatty acid oxidation. To determine if hyperoside's inhibition of LIPIN1 also affects TG synthesis, we conducted LC-MS based lipidomics assays to analyze serum TG levels. The OPLS-DA results showed that the R2X, R2Y, and Q2 values were 0.594, 0.841, and 0.41, indicating significant difference between the model group and the hyperoside-treated group (data was not shown). Using a threshold value of $P < 0.05$ and a fold change greater than 1.3, we identified fifty-four lipids, comprising 11 upregulated and 43 downregulated lipids, between the model and hyperoside treatment groups. After hyperoside treatment, the serum levels of 18 TG, including (18:3/18:2/16:0), (18:2/16:1/16:0), (18:2/18:2/14:0), (18:2/16:0/16:0), (49:3), (17:1/17:1/17:1), (54:6), (47:2), (51:5), (18:2/18:1/16:0), (18:1/18:1/16:0), (16:1/16:0/16:0), (45:2), (54:2), (48:0), (53:1), (56:7), and (47:3) in NAFLD rats were significantly decreased. Additionally, DG(18:2/16:1/0:0) and 11 MSDGs, including (O-26:0/14:0), (O-26:1/14:0), (O-26:2/16:0), (O-22:1/16:0), (O-28:3/16:0), (O-26:1/16:0), (O-27:0/16:0), (O-11:0/24:0), (O-28:0/18:1), (O-28:0/17:0), and (O-26:1/18:1) in NAFLD rats were also significantly elevated by hyperoside treatment, the details are shown in Fig. 5H and Table.S1. These findings demonstrate that hyperoside can inhibit the expression of LIPIN1 by activating FXR, thereby inhibiting TG synthesis and reducing TG levels in the organism.

Hyperoside inhibits ACLY independently of FXR, thereby suppressing fatty acid synthesis

In the TMT-based proteomic analysis, hyperoside significantly downregulated the expression of ACLY, an essential enzyme that bridges carbohydrate metabolism to lipid metabolism by converting citrate into acetyl-CoA for fatty acid and cholesterol biosynthesis. To confirm whether ACLY is a direct target of hyperoside, we employed molecular docking, ITC, WB, and other techniques. The molecular docking results showed that stable hydrogen bonds formed between hyperoside and the specific amino acid residues of ACLY, including GLY380, AG378, GLY341, GLY342, THR353, ALA280, MET278, and ALA310, with a binding energy –8.9 kcal/mol (Fig. 6A). Molecular dynamics simulations were conducted to evaluate the interaction between ACLY and hyperoside. As shown in Fig. 6B, the RMSD of the protein increased rapidly before 10 ns, reaching a maximum value of 17.5 Å, and then continued to increase slowly between 10 ns and 60 ns before stabilizing after 60 ns. Meanwhile, the RMSD of the ligand followed a similar overall trend but remained relatively stable within 10 Å. Analysis of the protein's RMSF revealed that it remained relatively stable up to the VAL821 region, after which the fluctuations increased (PDB ID: 8G5D, which includes chains A, B, C, and D; the D chain was selected for molecular docking) (Fig. 6C). The radius of gyration (RG) was calculated with the protein as the primary structure (Fig. 6D). Notably, the RG of the protein fluctuated significantly before 25 ns but remained stable within 2 Å between 25 ns and 100 ns, with the protein conformation stabilized. WB analysis also confirmed that hyperoside downregulated hepatic ACLY expression levels. ITC analysis revealed that hyperoside exhibits a significantly higher binding affinity to ACLY, with a dissociation constant (Ka) of $2.26e^4\ M^{-1}$, as illustrated in Fig. 6E. Additionally, hyperoside suppressed ACLY expression in the liver and effectively attenuated the palmitic acid-induced elevation of ACLY levels in AML12 cells. (Fig. 6G). To further explore whether the inhibition of ACLY by hyperoside is mediated by FXR activation, HepG2 and AML12 cell lines were treated to GW4064, a pan-FXR agonist. The results in Fig. 6G indicate that while GW4064 activated FXR in both cell lines, it did not affect ACLY protein levels. Collectively, these findings suggest that ACLY may be a direct target of hyperoside. ACLY is a key enzyme in fatty acid synthesis and plays a crucial role in hepatic lipid accumulation, with free fatty acids being significant contributors to this process. We determined the total fatty acid content in the liver and found that hyperoside significantly reduced this content. Additionally, high-resolution mass spectrometry was used to quantify medium- and short-chain fatty acids in the liver. The results indicated that hyperoside administration decreased all 41 detected fatty acids (Fig. 6F), including 10 monounsaturated fatty acids (MUFAs), 14 saturated fatty acids (SFAs),15 polyunsaturated fatty acids (PUFAs), and 2 trans unsaturated fatty acids (TUFAs). Furthermore, the levels of MUFAs, PUFAs, SFAs, and TUFAs were significantly reduced following hyperoside treatment (Fig. 6I). The one-way ANOVA test indicated that 16 fatty acids were significantly decreased ($P < 0.05$ and $FC > 1.2$) in the liver post- hyperoside treatment compared to the model group

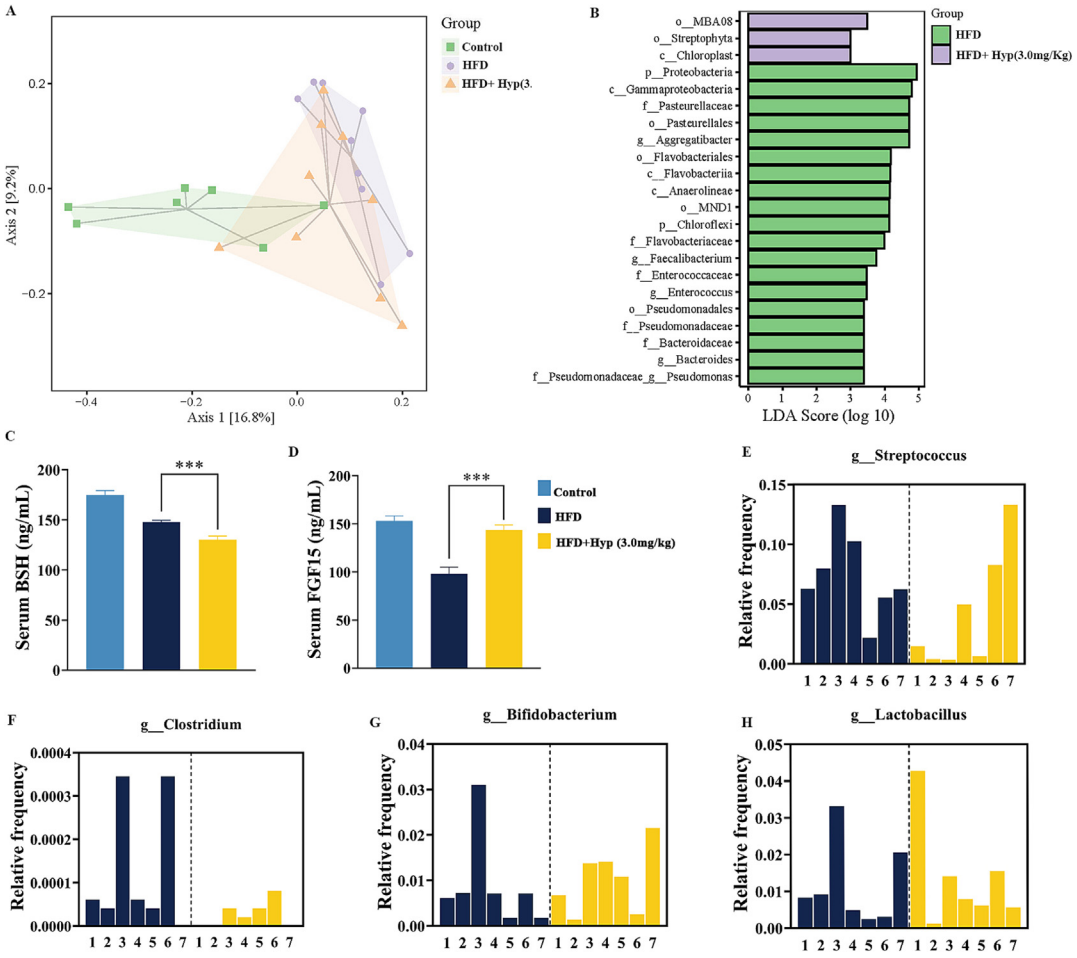

Fig. 4. Hyperoside reshaped the gut microbiota in NAFLD rats. A. Jaccard based Non-metric Multidimensional Scaling (NMDS) analysis with hull between control, HFD, and hyperoside groups, n = 7 individuals/group. B. LEfSe analysis between HFD, and hyperoside groups, n = 7 individuals/group. C-D. Hyperoside increased the levels of BSH and FGF15 in the serum of NAFLD rats. E-H. The microbial with BSH enzyme activity in the ileal contents of rat treated with HFD and hyperoside. Data were expressed as mean ± SEM. Differences of data in rats were assessed by the One-way ANOVA test, respectively, *** $P < 0.001$.

(Fig. 6J), including 8 SFAs(tetracosanoic acid, tricosanoic acid, docosanoic acid, nonadecanoic acid, heptadecanoic acid, heneicosanoic acid, pentadecanoic acid, eicosanoic acid), 3 MUFAs (12Z-Heneicosenoic acid, 13Z-Docosenoic acid, oleic acid), 4 PUFAs(arachidonic acid, docosahexaenoic acid DHA, alpha_Linolenic acid, 8,11,14_Eicosatrienoic acid), 1 TUFAs(10E-Nonadecenoic acid). Consistent with the protein expression of SCD1, the rate-limiting enzyme in monounsaturated fatty acid synthesis, hyperoside intervention decreased fatty acid synthesis. These results suggest that hyperoside inhibits SCD1 activity through FXR activation and directly suppresses ACLY protein expression, working synergistically to inhibit fatty acid synthesis and reduce lipid accumulation in the liver.

Discussion

Hyperoside has demonstrated a range of potent pharmacological properties, including antidiabetic, antithrombotic, anti-inflammatory, antifungal, antiviral, antioxidative, and hepatoprotective effects[26]. Our previous study was the first to show that hyperoside treatment significantly reduces hepatic cholesterol and triglyceride levels, which are linked to bile acid metabolism [25]. In this study, hyperoside was found to reduce BAs levels, promote fatty acid oxidation, and decrease lipid synthesis by activating FXR. Additionally, it increased conjugated BAs by inhibiting the activity of intestinal BSH bacteria, inhibited ACLY protein activity, and synergistically inhibited BAs and fatty acid synthesis with FXR, thereby exerting an anti-NAFLD effect.

Numerous studies have substantiated the role of BAs metabolism in NAFLD, highlighting its interaction with nuclear receptors and subsequent modulation of TG and cholesterol homeostasis [27,28]. In our study, hyperoside treatment significantly reduced the BAs biosynthesis in the livers of rats afflicted with NAFLD, thereby mitigating BAs induced hepatic toxicity [25]. In addition, our observations indicate that hyperoside enhances excretion of BAs from hepatic to intestinal. This effect is mediated by the upregulation of proteins such as BSEP, which consequently mitigates the hepatic accumulation of BAs and lipids [29,30]. Intriguingly, proteomic analysis utilizing TMT labeling revealed a significant upregulation in the expression of flavin-containing monooxygenase 5 (Fmo5), an enzyme involved in taurine synthesis[31], as well as bile acid CoA: amino acid N-acyltransferase (BAAT) following hyperoside treatment, suggesting that hyperoside also augments the production of conjugated BAs by stimulating the activity of both BAAT and Fmo5.

We observed notable differences in BAs metabolism between humans and rodents. In humans, cholic and chenodeoxycholic acids are the primary BAs, whereas rodents produce muricholic acids due to alternative hydroxylation. Approximately half of the BAs pool in mice consists of 6-hydroxylated muricholic acids,

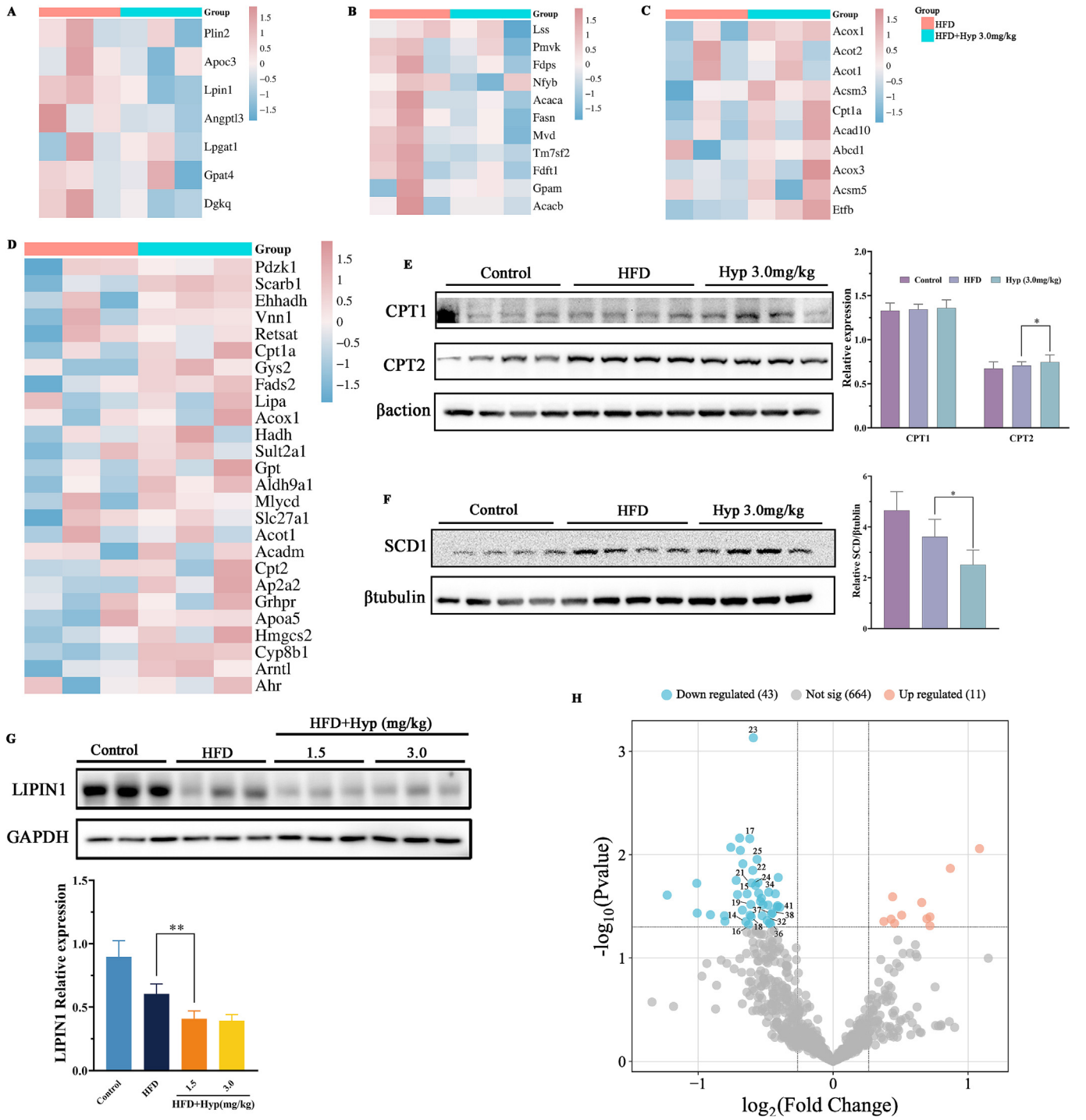

Fig. 5. Hyperoside activates FXR, thereby suppressing fatty acid and triglyceride synthesis and enhancing fatty acid oxidation in the livers of rats with NAFLD. The expression profile of triglyceride synthesis proteins(A), AMPK target proteins(B), fatty acid degradation related proteins(C), and fatty acid oxidation related proteins (D)was presented as a clustered heatmap. E. The protein expression of hepatic CPT1and CPT2 that involved in fatty acid oxidation was significantly increased by hyperoside. F. The protein expression of hepatic SCD1was inhibited by hyperoside. G. The protein expression of hepatic LIPIN1was inhibited by hyperoside. H. Volcano map of differential serum lipids between HFD and hyperoside groups. FC > 1.2 or < 0.83, and P < 0.05. Data were expressed as mean ± SEM. Differences of data in rats were assessed by the One-way ANOVA test, respectively, $^{*}P < 0.05$, $^{**}P < 0.01$.

which may mitigate the effects of hydrophobic BAs such as cholic acid, chenodeoxycholic acid, and deoxycholic acid. Additionally, the gut microbiota in both species further diversifies the BA spectrum, contributing to differences in secondary BAs [32,33].

Disruption of the enterohepatic circulation has a more pronounced effect on cholesterol metabolism and LDL levels in humans. The hydrophobicity of individual BAs influences biliary lipid secretion and fat absorption. BAs toxicity is primarily linked to their hydrophobicity; for example, more hydrophilic BAs like glycoursodeoxycholic acid, glycochenodeoxycholic acid, and taurodeoxycholic acid are less toxic [34,35]. Hyperoside has been shown to promote the formation of conjugated BAs, increasing their water solubility and reducing hepatotoxicity.

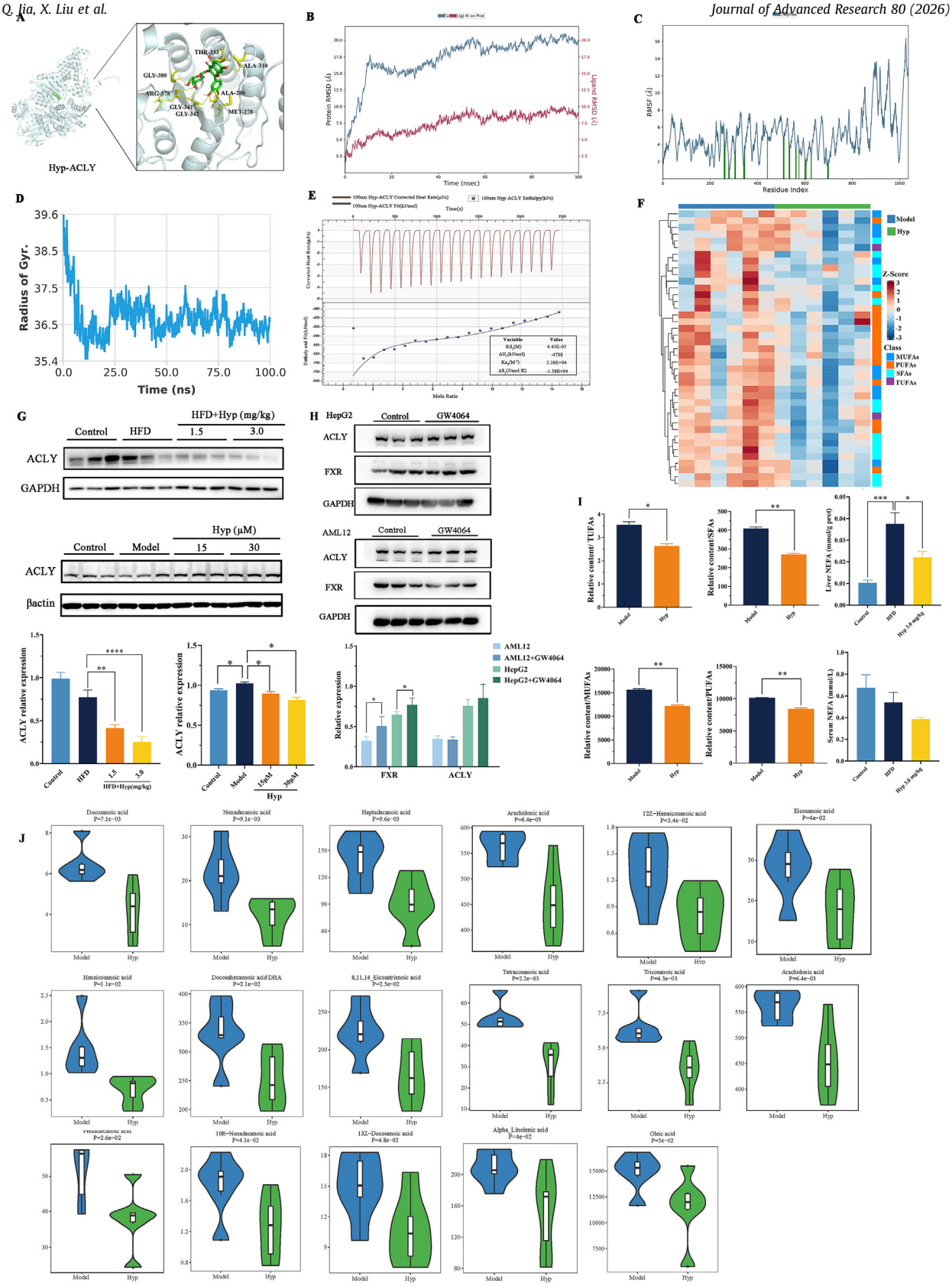

Fig. 6. Hyperoside inhibits fatty acid synthesis by inhibiting ACLY, independently of FXR. A. The stable hydrogen bonds formed between hyperoside and the specific amino acid residues GLY380, AG378, GLY341, GLY342, THR353, ALA280, MET278, ALA310 of the ACLY, providing specific binding energy –8.9 kcal/mol. B. Trend of root mean square difference (RMSD) plots for ACLY and hyperoside complexes. C.Root Mean Square Swing (RMSF) chart trend for ACLY. D. ACLY's radius of gyration (RG) chart trend. E. ITC analysis of ACLY with hyperoside. Heat flow as a function of time (red) and the blue dotted line corresponds to the theoretical independent model. The thermodynamic constants are presented in the pane. G-H. Hyperoside inhibited protein expression of hepatic ACLY, and reversed the elevated ACLY protein induced by oleic acid/palmitic acid in AML12 cell lines. F. Heatmap represented the expression profile of all detected fatty acids in the comparison of hyperoside treatment and HFD groups. I. hyperoside significantly reduced the subclasses of fatty acids in both the serum and liver of NAFLD rats. J. The expression profile of differentially fatty acids ($P < 0.05$ and $FC > 1.2$) identified in the comparison of hyperoside treatment and HFD groups. Data were expressed as mean ± SEM. Differences of data for mice and human subjects were assessed by the One-way ANOVA test, respectively, $^{*}P < 0.05$, $^{**}P < 0.01$, $^{***}P < 0.001$. (For interpretation of the references to colour in this figure legend, the reader is referred to the web version of this article.)

Mice primarily produce taurine conjugates of BAs, while humans predominantly produce glycine conjugates, with some taurine conjugates. In rats, hyperoside facilitates taurine conjugation of BAs, enhancing their hydrophilicity and reducing hepatotoxicity [36]. However, further clinical data are needed to determine whether hyperoside can similarly increase the level of glycine-conjugated BAs in humans.

Previous studies have shown that intestinal microbes produce BSH, an enzyme that catalyzes the conversion of conjugated BAs into their unconjugated forms [37,38]. Our prior research has shown that hyperoside increases the levels of conjugated BAs in rat livers [25]. Previous studies have identified that diminished BSH activity primarily results from a decreased relative abundance of specific bacterial genera, including *Lactobacillus*, *Bifidobacteria*, *Bacillus*, *Streptococcus*, *Bacteroides*, *Clostridium*, and *Enterococcus* [28,39]. In our study, hyperoside treatment was linked to a reduced relative abundance of the genera *Bacteroides*, *Enterococcus*, *Lactobacillus*, *Bifidobacteria*, *Bacillus*, and *Streptococcus* genera in the intestine. Moreover, hyperoside treatment significantly diminished the levels of BSH in the intestinal tract of rats. Consequently, the observed elevation of conjugated BAs in the liver and intestine following hyperoside administration may stem from a synergistic reduction of BAAT activity in the liver coupled with a decrease in intestinal bacterial BSH populations. Additionally, there is substantial evidence indicating the toxicity of hydrophobic BAs; for instance, increased exposure to these compounds can activate necrosis and apoptosis pathways. In contrast, conjugated BAs are more hydrophilic and exhibit lower cytotoxic effects compared to their unconjugated counterparts. Hyperoside targets FXR to reduce BAs synthesis, promote conjugated BAs synthesis, and inhibit their degradation in the intestine, thereby increasing conjugated BAs levels in NAFLD rats.

Traditionally, BAs have been identified as endogenous ligands for FXR, playing a crucial role in regulating lipid metabolism and aiding in the prevention and management of NAFLD [40,41]. Among reported FXR receptor BAs agonists, hyperoside increased the intestinal levels of TCA, TDCA, TLCA, GCA, GDCA, CDCA, and DCA in NAFLD rats. This elevation in BAs likely contributes to the upregulated expression of FXR protein observed in the intestine and liver [42–44]. In the current study, we noted an increase in the levels of total conjugated BAs within the intestine following hyperoside treatment, corroborating our previous findings that hyperoside enhances the concentration of these BAs in the liver of rats [25]. BAs function not only as signaling molecules but also as endogenous ligands for FXR. When activated, intestinal FXR promotes the production of fibroblast growth factor 15 (FGF15), which interacts with other FGFs to initiate a cascade that ultimately downregulates hepatic BAs synthesis from cholesterol [45] and an increased level of FGF15 in the serum was also observed in the hyperoside treatment group (Fig. 4D). The induction of intestinal FXR by hyperoside may confer therapeutic benefits in NAFLD by attenuating systemic inflammation and reducing hepatic glucose production [46].

The activation of FXR is crucial in the regulation of BAs metabolism and plays a significant role in NAFLD [47]. However, recent clinical studies have revealed that FXR activation may also lead to side effects, including elevated serum total cholesterol and low-density lipoprotein cholesterol (LDL-c), which can result in disruptions of cholesterol metabolism. Hence, the challenge of activating FXR to intervene in NAFLD while avoiding these side effects has become a critical topic in this field. Importantly, ACLY is instrumental in the production of acetyl-CoA, which serves as a precursor for cholesterol synthesis. In this study, we found that hyperoside could directly inhibit ACLY, thereby reducing acetyl-CoA and consequently decreasing cholesterol synthesis, in addition to reducing the synthesis of fatty acids and lipids. Using metabolomics techniques, we confirmed that hyperoside could inhibit ACLY and reduce the production of fatty acids, such as oleic acid, a major component of triglycerides. Consequently, dual-target drugs that act on both FXR and ACLY, as discussed in this study, could provide new avenues for the development of NAFLD therapies.

Over the past 20 years, the theoretical hypothesis of NAFLD pathogenesis has evolved from the "two-hit theory" to the "multiple-hit model." Liver TG accumulation is considered to be the "initial trigger"[6]. Hepatic TG levels depend largely on the uptake of free fatty acids, *de novo* lipogenesis, fatty acid oxidation, and VLDL secretion. NAFLD develops when the liver fails to adequately compensate for the increased uptake of circulating fatty acids and the *de novo* synthesis of lipids [7,8,48,49,50]. Dietary carbohydrates are a significant source of fatty acid synthesis, as the liver converts glucose into fatty acids through a process called *de novo* lipogenesis. The initial step of this pathway is catalyzed by ACLY, which converts citrate derived from the tricarboxylic acid (TCA) cycle into cytosolic acetyl-CoA, a key precursor for *de novo* lipogenesis [51]. Within hepatocytes, fatty acids can either undergo oxidation or be re-esterified into glycerolipids and phospholipids. Acyl-CoAs generated by ACSL1 in the mitochondrial outer membrane are destined for β-oxidation by CPT1, CPT2, and other enzymes[52]. Therefore, ACLY is crucial nodes in fatty acid metabolism, and targeting ACLY to address fatty acid metabolism disorders may lay the foundation for novel therapeutic strategies to alleviate NAFLD [50,51]. In our experiments, hyperoside significantly inhibited hepatic ACLY activity in rats, reducing the availability of citrate for FAs and cholesterol biosynthesis [53]. Furthermore, the activities of CPT1 and CPT2 exhibited a significant increase, indicating the acceleration effect of hyperoside treatment on β-oxidation. Our findings imply that hyperoside attenuates *de novo* lipogenesis by suppressing FAs synthesis and enhancing the β-oxidation of FAs.

In liver tissue, FAs from the plasma are incorporated into TG [54]. Interestingly, in the current study, serum long chain fatty acids levels were elevated in hyperoside-treated NAFLD rats, despite the low levels of TG in the liver. To further investigate this phenomenon, we evaluated the levels of CD36, a critical fatty acid translocase, in both hepatic and intestinal tissues using TMT-based proteomics analysis. The data revealed that hyperoside reduced the expression of CD36 in the liver. Consequently, it appears that hyperoside may diminish fatty acid uptake by modulating the activity of fatty acid transport proteins. Hyperoside has a diverse impact on NAFLD by not only inhibiting fatty acid absorption and TG synthesis but also promoting fatty acid oxidation, reducing fatty acid synthesis, and decreasing fatty acid transport. This multifaceted action plays a crucial role in alleviating NAFLD [55].

Lipin 1 plays a crucial role in regulating lipid metabolism in hepatic cells by catalyzing the dephosphorylation of phosphatidic acid to generate diacylglycerol. Ethanol exposure induces a marked increase in lipin 1 expression, leading to enhanced PAP activity and subsequent lipid accumulation in the livers of mice on an ethanol diet [56–58]. Our lipidomic analysis revealed that hyperoside treatment significantly reduced the serum concentrations of various TG species. Notably, hepatic lipin 1 expression was decreased in hyperoside-treated mice fed HFD, whereas DGAT1 levels remained unchanged. These results suggest that hyperoside effectively lowers hepatic lipin1 levels, thereby diminishing diacylglycerol synthesis and reducing hepatic lipid deposition.

To further verify whether the inhibition of ACLY by hyperoside is related to the activation of FXR, HepG2 and AML12 cell lines were subjected to GW4064, a pan-FXR agonist, in an in vitro assay. The findings revealed that while GW4064 activated FXR in both cell lines, it did not alter ACLY protein levels. These findings substantiate the mechanism by which hyperoside mitigates NAFLD in mice, which involves FXR activation and ACLY inhibition.

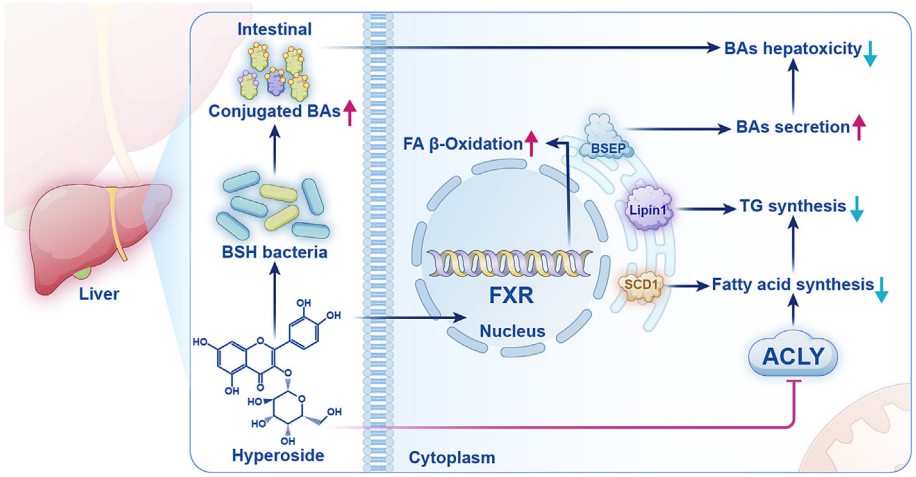

Fig. 7. Proposed mechanism for Hyperoside alleviate NAFLD in rats. Hyperoside promoted BAs synthetic pathway by simultaneous activation of hepatic FXR and inhibition of ACLY, accompanied by the inhibition of *de novo* lipogenesis, the promotion of fatty acid oxidation, and the facilitation of BA excretion. Hyperoside induced the accumulation of conjugated BAs in ileum by inhibiting BSH bacteria.

Conclusions

In summary, Fig. 7 illustrates the multifaceted mechanism by which hyperoside mitigates NAFLD, encompassing several key factors: (1) Hyperoside directly activates FXR, inhibiting *de novo* lipogenesis by suppressing SCD1 and SREBP1 and promoting fatty acid oxidation. (2) Activation of FXR by hyperoside promotes the secretion of BAs from the liver to the intestine, accompanied by a reduced abundance of BSH-producing microbes, leading to an increase in conjugated BAs. (3) Hyperoside inhibits the protein activity of ACLY, working in conjunction with FXR to inhibit the endogenous synthesis of fatty acids.

Despite the strengths of this study, several limitations remain. After hyperoside inhibits ACLY, it is crucial to determine whether there is a significant difference in the acetyl-CoA content between mitochondria and the endoplasmic reticulum. Furthermore, elucidating the specific mechanism by which hyperoside inhibits ACLY to suppress fatty acid and cholesterol synthesis is essential. Additionally, the impact of hyperoside's metabolic behavior as a flavonoid glycoside compound on drug efficacy within the organism must be evaluated. Moreover, more clinical trials are required to assess the potential long-term side effects of hyperoside.

Ethics statement

The animal study was approved by The Animal ethics committee of Shandong First Medical University (No. S6066) and performed in accordance with the principles of the Animal ethics committee.

Compliance with ethics requirements

Animal studies were reported in compliance with the ARRIVE guidelines. All experimental procedures were approved by the Ethics Committee in college of pharmacy, Shandong first medical University (No. S6006). All experiments in this study were conducted according to the national legislation, the guidelines of the laboratory animal center at Shandong first medical University, and the Guide for the Care and Use of Laboratory Animals from the National Institutes of Health (the eighth edition).

CRediT authorship contribution statement

Songsong Wang: Conceptualization, Methodology, Data curation, Validation, Writing – original draft, Writing – review & editing. **Qiang Jia:** Conceptualization, Methodology, Data curation, Validation. **Xiaoli Liu:** Data curation, Validation. **Yihan Ma:** Data curation. **Ying Yang:** Data curation. **Xue Rong:** Methodology, Data curation. **Yang Wang:** Methodology, Data curation. **Haiyang Wang:** Methodology, Data curation. **Fusheng Liu:** Methodology, Data curation. **Shenshen Yang:** Methodology, Data curation. **Yubo Li:** Conceptualization, Supervision. **Liwen Han:** Conceptualization, Supervision, Writing – review & editing, Funding acquisition.

Declaration of competing interest

The authors declare that they have no known competing financial interests or personal relationships that could have appeared to influence the work reported in this paper.

Acknowledgements

This work was supported by the National Natural Science Foundation of China (No. 82404721) (No. 82474217), the Natural Science Foundation of Shandong province (ZR2024QH063), Academic Promotion Program of Shandong First Medical University (No. 2019LJ003), Innovation Team of Shandong Higher School Youth Innovation Technology Program (No. 2024KJJ032), the Traditional Chinese Medicine Science & Technology Project (No. M-2023149) (No. M20241701), and the foundation of New 20 University Policies of Jinan (No. 202333018), Scientific Research Fund Project of Shandong University of Traditional Chinese Medicine (No. KYZK2024Q32).

Appendix A. Supplementary material

Supplementary data to this article can be found online at https://doi.org/10.1016/j.jare.2025.05.014.

References

[1] Song N, Xu H, Wu S, Luo S, Xu J, Zhao Q, et al. Synergistic activation of AMPK by AdipoR1/2 agonist and inhibitor of EDPs-EBP interaction recover NAFLD through enhancing mitochondrial function in mice. Acta Pharm SinB 2023;13:542–58. doi: https://doi.org/10.1016/j.apsb.2022.10.003.

[2] Li X, Ge J, Li Y, Cai Y, Zheng Q, Huang N, et al. Integrative lipidomic and transcriptomic study unravels the therapeutic effects of saikosaponins A and D on non-alcoholic fatty liver disease. Acta Pharm SinB 2021;11:3527–41. doi: https://doi.org/10.1016/j.apsb.2021.03.018.

[3] Chen F, Esmaili S, Rogers GB, Bugianesi E, Petta S, Marchesini G, et al. Lean NAFLD: a distinct entity shaped by differential metabolic adaptation. Hepatology 2020;71:1213–27. doi: https://doi.org/10.1002/hep.30908.

[4] Zhou F, Zhou J, Wang W, Zhang XJ, Ji YX, Zhang P, et al. to 2018: A Systematic Review and Meta-Analysis. Hepatology7 2008;70(2019):1119–33. doi: https://doi.org/10.1002/hep.30702.

[5] Zhao Y, Xia T, Qiang X, Wang Y, Kang C, Meng Y, et al. Zhenjiang aromatic vinegar prevents the alcohol liver disease in mice via autophagy. eFood 2023;4:e118. doi: https://doi.org/10.1002/efd2.118.

[6] Friedman SL, Neuschwander-Tetri BA, Rinella M, Sanyal AJ. Mechanisms of NAFLD development and therapeutic strategies. Nat Med 2018;24:908–22. doi: https://doi.org/10.1038/s41591-018-0104-9.

[7] Sun R, Kang X, Zhao Y, Wang Z, Wang R, Fu R, et al. Sirtuin 3-mediated deacetylation of acyl-CoA synthetase family member 3 by protocatechuic acid attenuates non-alcoholic fatty liver disease. Brit J Pharmacol 2020;177:4166–80. doi: https://doi.org/10.1111/bph.15159.

[8] Goedeke L, Bates J, Vatner DF, Perry RJ, Wang T, Ramirez R, et al. Acetyl-CoA carboxylase inhibition reverses NAFLD and hepatic insulin resistance but promotes hypertriglyceridemia in rodents. Hepatology 2018;68:2197–211. doi: https://doi.org/10.1002/hep.30097.

[9] Tacke F, Weiskirchen R. Non-alcoholic fatty liver disease (NAFLD)/non-alcoholic steatohepatitis (NASH)-related liver fibrosis: mechanisms, treatment and prevention. Ann Transl Med 2021;9:729. doi: https://doi.org/10.21037/atm-20-4354.

[10] Powell EE, Wong VW-S, Rinella M. Non-alcoholic fatty liver disease. The Lancet 2021;397:2212–24. doi: https://doi.org/10.1016/S0140-6736(20)32511-3.

[11] Carr RM, Reid AE. FXR agonists as therapeutic agents for non-alcoholic fatty liver disease. Curr Atheroscler Rep 2015;17:500. doi: https://doi.org/10.1007/s11883-015-0500-2.

[12] Fang Y, Hegazy L, Finck BN, Elgendy B. Recent advances in the medicinal chemistry of farnesoid X receptor. J Med Chem 2021;64:17545–71. doi: https://doi.org/10.1021/acs.jmedchem.1c01017.

[13] Shi T, Wu L, Ma W, Ju L, Bai M, Chen X, et al. Nonalcoholic fatty liver disease: pathogenesis and treatment in traditional chinese medicine and western medicine. Evid-Based Compl Alt 2020:1–16. doi: https://doi.org/10.1155/2020/8749564.

[14] Ji L, Li Q, He Y, Zhang X, Zhou Z, Gao Y, et al. Therapeutic potential of traditional Chinese medicine for the treatment of NAFLD: A promising drug Potentilla discolor Bunge. Acta Pharm Sin1 2022;12:3529–47. doi: https://doi.org/10.1016/j.apsb.2022.05.001.

[15] Liao J, Luo J, Wang Y, Zhao J, Xie X, Qu F, et al. Advances in traditional Chinese medicine for liver disease therapy in 2021. Tradit Med Res 2022;7:58. doi: https://doi.org/10.53388/TMR20220219002.

[16] Fu K, Wang C, Ma C, Zhou H, Li Y. The potential application of chinese medicine in liver diseases: a new opportunity. Front Pharmacol 2021;12:771459. doi: https://doi.org/10.3389/fphar.2021.771459.

[17] Wang L, Yan Y, Wu L, Peng J. Natural products in non-alcoholic fatty liver disease (NAFLD): Novel lead discovery for drug development. Pharmacol Res 2023;196:106925. doi: https://doi.org/10.1016/j.phrs.2023.106925.

[18] Zhou H, Ma C, Wang C, Gong L, Zhang Y, Li Y. Research progress in use of traditional Chinese medicine monomer for treatment of non-alcoholic fatty liver disease. Eur J Pharmacol 2021;898:173976. doi: https://doi.org/10.1016/j.ejphar.2021.173976.

[19] Yan T, Yan N, Wang P, Xia Y, Hao H, Wang G, et al. Herbal drug discovery for the treatment of nonalcoholic fatty liver disease. Acta Pharm Sin B 2020;10:3–18. doi: https://doi.org/10.1016/j.apsb.2019.11.017.

[20] Zimmermann GR, Lehár J, Keith CT. Multi-target therapeutics: when the whole is greater than the sum of the parts. Drug Discov Today1 2007;12:34–42. doi: https://doi.org/10.1016/j.drudis.2006.11.008.

[21] He Q, Dong H, Guo Y, Gong M, Xia Q, Lu F, et al. Multi-target regulation of intestinal microbiota by berberine to improve type 2 diabetes mellitus. Front Endocrinol 2022;13:1074348. doi: https://doi.org/10.3389/fendo.2022.1074348.

[22] Ma JX, Yang W, Ng CYJ, Tang XD, Wong S, Gan RY, Zhong L. The hawthorn (Crataegus pinnatifida Bge.) fruit as a new dietary source of bioactive ingredients with multiple beneficial functions. Food Front 2024;5:1534–58. doi: https://doi.org/10.1002/fft2.413.

[23] Wang Q, Wei HC, Zhou SJ, Li Y, Zheng TT, Zhou CZ, et al. Hyperoside: a review on its sources, biological activities, and molecular mechanisms. Phytother Res3 2022;36:2779–802. doi: https://doi.org/10.1002/ptr.7478.

[24] Ai G, Huang Z. Acute toxicity and genotoxicity evaluation of hyperoside extracted from Abelmoschus manihot (L.) Medic. J Chin Pharm Sci. 2012;21. doi: https://doi.org/10.5246/jcps.2012.05.063.

[25] Wang S, Sheng F, Zou L, Xiao J, Li P. Hyperoside attenuates non-alcoholic fatty liver disease in rats via cholesterol metabolism and bile acid metabolism. J Adv Res 2021;34:109–22. doi: https://doi.org/10.1016/j.jare.2021.06.001.

[26] Raza A, Xu X, Sun H, Tang J, Ouyang Z. Pharmacological activities and pharmacokinetic study of hyperoside: a short review. Trop J Pharm Res 2017;16:2. doi: https://doi.org/10.4314/tjpr.v16i2.30.

[27] Houten SM, Watanabe M, Auwerx J. Endocrine functions of bile acids. EMBO J 2006;25:1419–25. doi: https://doi.org/10.1038/sj.emboj.7601049.

[28] Huang F, Zheng X, Ma X, Jiang R, Zhou W, Zhou S, et al. Theabrownin from Pu-erh tea attenuates hypercholesterolemia via modulation of gut microbiota and bile acid metabolism. Nat Commun. 2019;10:4791. doi: https://doi.org/10.1038/s41467-019-12896-x.

[29] Chen T, Zhou K, Sun T, Sang C, Jia W, Xie G. Altered bile acid glycine : taurine ratio in the progression of chronic liver disease. J Gastroenterol Hepatol 2022;37:208–15. doi: https://doi.org/10.1111/jgh.15709.

[30] Chen W, Wei Y, Xiong A, Li Y, Guan H, Wang Q, et al. Comprehensive analysis of serum and fecal bile acid profiles and interaction with gut microbiota in primary biliary cholangitis. Clin Rev Allergy Immunol 2020;58:25–38. doi: https://doi.org/10.1007/s12016-019-08731-2.

[31] Veeravalli S, Phillips IR, Freire RT, Varshavi D, Everett JR, Shephard EA. Flavin-containing monooxygenase 1 catalyzes the production of taurine from hypotaurine. Drug Metab Dispos 2020;48:378–85. doi: https://doi.org/10.1124/dmd.119.089995.

[32] Lorbek G, Lewinska M, Rozman D. Cytochrome P450s in the synthesis of cholesterol and bile acids-from mouse models to human diseases. FEBS J 2011;279:1516–33. doi: https://doi.org/10.1111/j.1742-4658.2011.08432.x.

[33] Zhang Z, Lv T, Wang X, Wu M, Zhang R, Yang X, et al. Role of the microbiota-gut-heart axis between bile acids and cardiovascular disease. Biomed Pharmacother 2024;174:116567. doi: https://doi.org/10.1016/j.biopha.2024.116567.

[34] Karsten REH, Gier K, de Meijer VE, Huibers WHC, Permentier HP, Verpoorte E, et al. Studying the intracellular bile acid concentration and toxicity in drug-induced cholestasis: comprehensive LC-MS/MS analysis with human liver slices. Toxicol. in Vitro 2025;104:106011. doi: https://doi.org/10.1016/j.tiv.2025.106011.

[35] Wang S, Li B, Tan H, Sun X, Tian J, Li S, et al. Cyanidin-3-O-glucoside magic: Unveiling the power to inhibit cholesterol absorption via the intestinal farnesoid X receptor-bile acids pathway with Lactobacillus Marvel. Food Front 2024;5:2721–36. doi: https://doi.org/10.1002/fft2.482.

[36] Tran QT, Sendler M, Wiese ML, Doller J, Zierke L, Gischke M, et al. Systemic bile acids affect the severity of acute pancreatitis in mice depending on their hydrophobicity and the disease pathogenesis. Int J Mol Sci 2022;23:13592. doi: https://doi.org/10.3390/ijms232113592.

[37] Zhang Y, Edwards PA. FXR signaling in metabolic disease. FEBS Lett 2008;582:10–8. doi: https://doi.org/10.1016/j.febslet.2007.11.015.

[38] Xu J, Xie S, Chi S, Zhang S, Cao J, Tan B. Protective effects of taurocholic acid on excessive hepatic lipid accumulation via regulation of bile acid metabolism in grouper. Food Funct 2022;13:3050–62. doi: https://doi.org/10.1039/D1FO04085E.

[39] Sayin SI, Wahlstrom A, Felin J, Jantti S, Marschall HU, Bamberg K, et al. Gut microbiota regulates bile acid metabolism by reducing the levels of tauro-beta-muricholic acid, a naturally occurring FXR antagonist. Cell Metab 2013;17:225–35. doi: https://doi.org/10.1016/j.cmet.2013.01.003.

[40] Zhu Y, Liu H, Zhang M, Guo GL. Fatty liver diseases, bile acids, and FXR. Acta Pharm Sin B. 2016;6:409–12. doi: https://doi.org/10.1016/j.apsb.2016.07.008.

[41] Watanabe M, Houten SM, Wang L, Moschetta A, Mangelsdorf DJ, Heyman RA, et al. Bile acids lower triglyceride levels via a pathway involving FXR, SHP, and SREBP-1c. J Clin Invest1 2004;113:1408–18. doi: https://doi.org/10.1172/JCI21025.

[42] Pushpass RG, Alzoufairi S, Jackson KG, Lovegrove JA. Circulating bile acids as a link between the gut microbiota and cardiovascular health: impact of prebiotics, probiotics and polyphenol-rich foods. Nutr Res Rev 2022;35:161–80. doi: https://doi.org/10.1017/S0954422421000081.

[43] Makishima M, Okamoto AY, Repa JJ, Tu H, Learned RM, Luk A, et al. Identification of a nuclear receptor for bile acids. Science. 1999;284:1362–5. doi: https://doi.org/10.1126/science.284.5418.1362.

[44] Wang H, Chen J, Hollister K, Sowers LC, Forman BM. Endogenous bile acids are ligands for the nuclear receptor FXR/BAR. Mol Cell 1999;3:543–53. doi: https://doi.org/10.1016/S1097-2765(00)80348-2.

[45] Inagaki T, Choi M, Moschetta A, Peng L, Cummins CL, McDonald JG, et al. Fibroblast growth factor 15 functions as an enterohepatic signal to regulate bile acid homeostasis. Cell Metab2 2005;2:217–25. doi: https://doi.org/10.1016/j.cmet.2005.09.001.

[46] Fang S, Suh JM, Reilly SM, Yu E, Osborn O, Lackey D, et al. Intestinal FXR agonism promotes adipose tissue browning and reduces obesity and insulin resistance. Nat Med 2015;21:159–65. doi: https://doi.org/10.1038/nm.3760.

[47] Li X, Wang H, Li Y, Huang M, Li X, Yu Z, et al. Pathologic and therapeutic insights into cholestatic liver disease-associated depressive disorder. Acta Materia Medica 2025;4:216–32. doi: https://doi.org/10.15212/AMM-2024-0082.

[48] Duan J, Wang Z, Duan R, Yang C, Zhao R, Feng Q, et al. Therapeutic targeting of hepatic ACSL4 ameliorates NASH in mice. Hepatology 2022;75:140–53. doi: https://doi.org/10.1002/hep.32148.

[49] Lambert JE, Ramos-Roman MA, Browning JD, Parks EJ. Increased de novo lipogenesis is a distinct characteristic of individuals with nonalcoholic fatty

liver disease. Gastroenterology 2014;146:726–35. doi: https://doi.org/10.1053/j.gastro.2013.11.049.
[50] Donnelly KL, Smith CI, Schwarzenberg SJ, Jessurun J, Boldt MD, Parks EJ. Sources of fatty acids stored in liver and secreted via lipoproteins in patients with nonalcoholic fatty liver disease. J Clin Invest 2005;115:1343–51. doi: https://doi.org/10.1172/JCI200523621.
[51] Morrow MR, Batchuluun B, Wu J, Ahmadi E, Leroux JM, Mohammadi-Shemirani P, et al. Inhibition of ATP-citrate lyase improves NASH, liver fibrosis, and dyslipidemia. Cell Metab 2022;34:919–36. doi: https://doi.org/10.1016/j.cmet.2022.05.004.
[52] Huh JY, Reilly SM, Abu-Odeh M, Murphy AN, Mahata SK, Zhang J, et al. TANK-binding kinase 1 regulates the localization of acyl-CoA synthetase ACSL1 to control hepatic fatty acid oxidation. Cell Metab 2020;32:1012–27. doi: https://doi.org/10.1016/j.cmet.2020.10.010.
[53] Schadinger SE, Bucher NL, Schreiber BM, Farmer SR. PPARgamma2 regulates lipogenesis and lipid accumulation in steatotic hepatocytes. Am J Physiol Endocrinol Metab 2005;288:1195–205. doi: https://doi.org/10.1152/ajpendo.00513.2004.
[54] Kawano Y, Cohen DE. Mechanisms of hepatic triglyceride accumulation in non-alcoholic fatty liver disease. J Gastroenterol 2013;48:434–41. doi: https://doi.org/10.1007/s00535-013-0758-5.
[55] Takeuchi K, Reue K. Biochemistry, physiology, and genetics of GPAT, AGPAT, and lipin enzymes in triglyceride synthesis. Am J Physiol Endocrinol Metab 2009;296:1195–2209. doi: https://doi.org/10.1152/ajpendo.90958.2008.
[56] Hu M, Wang F, Li X, Rogers CQ, Liang X, Finck BN, et al. Regulation of hepatic lipin-1 by ethanol: role of AMP-activated protein kinase/sterol regulatory element-binding protein 1 signaling in mice. Hepatology 2012;55:437–46. doi: https://doi.org/10.1002/hep.24708.
[57] Xu X, So JS, Park JG, Lee AH. Transcriptional control of hepatic lipid metabolism by SREBP and ChREBP. Semin Liver Dis 2013;33:301–11. doi: https://doi.org/10.1055/s-0033-1358523.
[58] Donkor J, Sariahmetoglu M, Dewald J, Brindley DN, Reue K. Three mammalian lipins act as phosphatidate phosphatases with distinct tissue expression patterns. J Biol Chem 2007;282:3450–7. doi: https://doi.org/10.1074/jbc.M610745200.